Electronic Supplementary Material (ESM) 1 of

Validation of a two-layer depth-averaged model by comparison with an experimental dilute stratified pyroclastic density current

Hiroyuki A. Shimizu[1]*, **Takehiro Koyaguchi**[2], **Yujiro J. Suzuki**[2], **Ermanno Brosch**[3], **Gert Lube**[3], **Matteo Cerminara**[4]

[1]National Research Institute for Earth Science and Disaster Resilience, 3-1 Tennodai, Tsukuba, Ibaraki 305-0006, Japan

[2]Earthquake Research Institute, The University of Tokyo, 1-1-1 Yayoi, Bunkyo-ku, Tokyo 113-0032, Japan

[3]Volcanic Risk Solutions, Massey University, Private Bag 11 222, Palmerston North, New Zealand

[4]Istituto Nazionale di Geofisica e Vulcanologia, Sezione di Pisa, Via della Faggiola 32, 56126 Pisa, Italy

*Corresponding author:

E-mail address: s-hiro@bosai.go.jp; ORCID iD: 0000-0001-6559-9331

Supplementary Information

We first summarize the contents of this ESM (i.e., ESM 1) and the other ESMs.

ESM	Contents
1 (.pdf)	**Supplementary Information S1:** Definition of benchmark of numerical models for dilute stratified PDCs **Supplementary Information S2:** Validation of the hindered-settling model for a dense underflow
2 (.xlsx)	Estimations of mean density of solid particles (ρ_s) and mean terminal velocity of particles (W_T) from the experimental data at Profile 1
3 (.mov)	**Supplementary Movie 1:** Two-layer PDC model with input parameter values in Table 1 (i.e., Run Best-fit)
4 (.mov)	**Supplementary Movie 2:** Two-layer PDC model with the same parameters as for the Run Best-fit (Movie 1) except for $W_{sH} = 5.9 \times 10^{-1}$ m/s (i.e., Run Reference)
5 (.mov)	**Supplementary Movie 3:** Basal-layer model where the settling speed W_{sH} is set to 7.3×10^{-3} m/s explained by the hindered-settling model (Table S4 gives input parameter values)

S1. Definition of benchmark of numerical models for dilute stratified PDCs

This Supplementary Information defines a benchmark of numerical models for dilute stratified PDCs on the basis of a large-scale experiment conducted at the eruption simulator PELE. The experiment generated a PDC through the gravitational collapse of a suspension of particles and air into an instrumented run-out section (Brosch and Lube 2020). At a run-out distance of 3.12 m after the impact of the suspension onto the run-out section (defined as $x = 0$ in the main text), the characteristic gravity current structure was fully developed, comprising a thick suspended-load region (with the gravity current head, body, and wake regions) above a basal thin bed-load region (cf. Figs. 2 and 6 of Brosch and Lube 2020). In this benchmark, the experimental flow profiles at $x = 0$ (referred to as Profile 1 in the main text) are provided as the inlet flow conditions for numerical models. The experimental flow profiles in distal areas ($x > 0$), particularly at $x = 2.65$ and 7.78 m (referred to as Profiles 2 and 3 in the main text), are provided for comparison with the numerical results.

The experimental flow profiles at each point (i.e., Profiles 1, 2, and 3) are obtained through time (t)- and height (z)-variant measurements of the following flow properties: flow velocity, flow temperature, flow particle volume fraction, and flow grain size distribution. To allow the benchmarking of PDC models with a range of levels of complexity (e.g., transient 2D/3D models, stationary 2D/3D models, transient two-layer depth-averaged 1D models, stationary two-layer depth-averaged 1D models, and other integral models), the experimental flow profiles are expressed as mathematical functions in time-dependent or time-averaged and depth-dependent or two-layer depth-averaged forms. These forms of Profiles 1, 2, and 3 are summarized in Tables S1, S2, and S3, respectively. Here the flow velocity function U,

$$U(z,t) = U_{\max}(z/z_{\mathrm{u}})^{\xi} \exp\left[-\left(\frac{z/z_{\mathrm{u}} - 1}{\chi}\right)^2 - \xi(z/z_{\mathrm{u}} - 1)\right], \quad \text{(S1)}$$

and the flow body thickness function H,

$$H(t) = z_{\mathrm{u}}(\chi + 1), \quad \text{(S2)}$$

are used, where $U_{\max}$ is the maximum velocity, z_{u} is the maximum velocity height, ξ is the wall exponent, and χ is the outer layer thickness. See Cerminara et al. (2021) for details of the derivation of the mathematical functions.

This paper uses the time- and depth-averaged forms of Profiles 1, 2, and 3 (see Tables S1, S2, and S3). For the present purpose of estimating the value of W_{sH}, it is particularly important to assess the uncertainties in experimentally observed values of ϕ_{sH}, h_{H1}, and u_{H1}. On the basis of the measurements of the time-variant volume of deposited mass entering the samplers and the PIV analyses, the solid volume fraction of the bed load is estimated to be of order 10^{-2} (Brosch and Lube 2020); we consider a range of solid volume fractions in the bed load ($\phi_{\mathrm{sH}} = 0.01$–$0.05$). The time-series data of the bed-load thickness at Profile 1 ($x = 0$) shows that the time-averaged bed-load thickness at $x = 0$ (i.e., h_{H1}) was about 0.005–0.02 m (see Fig. S1a). These observations along with the time-averaged height-dependent fitting function of flow velocity at Profile 1 (i.e., Eq. (S1)) give the time- and depth-averaged velocity (see Fig. S1b); the depth average between heights 0 and h_{H1} yields $u_{\mathrm{H1}} = 2.36$–3.27 m/s (Table S1).

Table S1 Experimental flow profiles at $x = 0$ m (i.e., Profile 1) expressed as mathematical functions in time-dependent or time-averaged and depth-dependent or two-layer depth-averaged forms

Profile 1	Time (t)-dependent			Time-averaged		
	Depth (z)-dependent	Depth-averaged		Depth (z)-dependent	Depth-averaged	
		Suspended load	Bed load		Suspended load	Bed load
Velocity [m/s]	Eq. (S1) with $U = 6.378 + 1.267t - 0.455t^2 - 0.0001049t^3$, $z_{\mathrm{u}} = 0.2142 + 0.03276t$, $\xi = 0.1662 + 0.04188t$, $\chi = 4.294 - 0.3661t$	$4.818 + 0.8409t - 0.316t^2 - 0.0007094t^3$	NOT available	Eq. (S1) with $U = 6.451$, $z_{\mathrm{u}} = 0.2751$, $\xi = 0.2374$, $\chi = 3.6$	4.8	3 (2.36-3.27)
Thickness [m]	---	Eq. (S2) with $z_{\mathrm{u}} = 0.2142 + 0.03276t$, $\chi = 4.294 - 0.3661t$	NOT available	---	1.265	0.015 (0.005-0.02)
Temperature [K]	NOT available	$283.85 + 11.16t - 36.3t^2 + 76t^3 - 91.03t^4 + 64.36t^5 - 26.53t^6 + 6.218t^7 - 0.767t^8 + 0.0386t^9$	NOT available	$303.9 \exp\left(-0.0942\left(\frac{z}{0.2751}\right)^{1.71}\right)$	292.29	
Particle mass fraction	NOT available	NOT available	NOT available	NOT available	0.4617	---
Particle volume fraction	NOT available	NOT available	NOT available	NOT available	---	0.02 (0.01-0.05)
Grain-size distribution	NOT available	NOT available	NOT available	NOT available	See ESM 2	

Table S2 Experimental flow profiles at $x = 2.65$ m (i.e., Profile 2) expressed as mathematical functions in time-dependent or time-averaged and depth-dependent or two-layer depth-averaged forms

Profile 2	Time (t)-dependent			Time-averaged		
	Depth (z)-dependent	Depth-averaged		Depth (z)-dependent	Depth-averaged	
		Suspended load	Bed load		Suspended load	Bed load
Velocity [m/s]	Eq. (S1) with $U = 4.433 + 2.242t - 1.085t^2 - 0.1154t^3$, $z_{\mathrm{u}} = 0.3215 - 0.01421t$, $\xi = 0.184 + 0.01803t$, $\chi = 3.6$	NOT available	NOT available	Eq. (S1) with $U = 4.969$, $z_{\mathrm{u}} = 0.2943$, $\xi = 0.218$, $\chi = 3.6$	NOT available	NOT available
Thickness [m]	---	Eq. (S2) with $z_{\mathrm{u}} = 0.3215 - 0.01421t$, $\chi = 3.6$	NOT available	---	1.35378	0.0146

Table S3 Experimental flow profiles at $x = 7.78$ m (i.e., Profile 3) expressed as mathematical functions in time-dependent or time-averaged and depth-dependent or two-layer depth-averaged forms

Profile 3	Time (t)-dependent			Time-averaged		
	Depth (z)-dependent	Depth-averaged		Depth (z)-dependent	Depth-averaged	
		Suspended load	Bed load		Suspended load	Bed load
Velocity [m/s]	Eq. (S1) with $U = 5.882 - 0.4119t - 0.2665t^2 + 0.04998t^3$, $z_u = 0.2721 - 0.003674t$, $\xi = 0.0622 + 0.116t$, $\chi = 3.6$	NOT available	NOT available	Eq. (S1) with $U = 4.436$, $z_u = 0.2795$, $\xi = 0.2943$, $\chi = 3.6$	NOT available	NOT available
Thickness [m]	---	Eq. (S2) with $z_u = 0.2721 + 0.003674t$, $\chi = 3.6$	NOT available	---	1.2857	0.00794

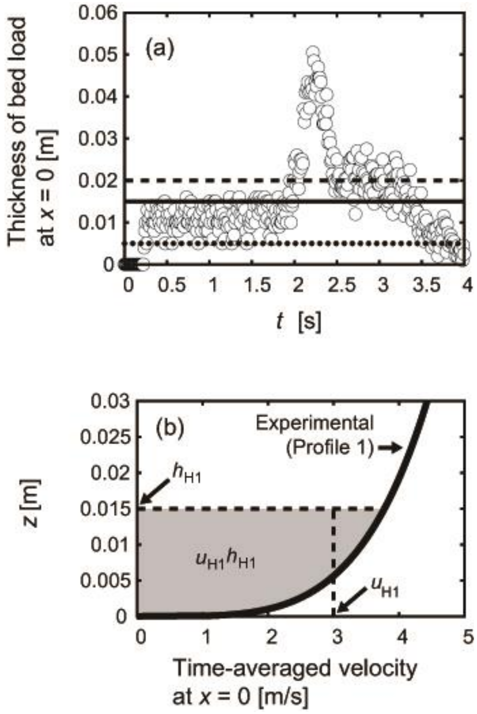

Fig. S1 (a) Thickness of bed load at Profile 1 ($x = 0$) as a function of time t. Circles represent data from the PELE experiment. Lines represent the values used in the numerical simulations (i.e., $h_{H1} = 0.005$ (dotted), 0.015 (solid), and 0.02 (dashed) m). (b) Time-averaged flow velocity at Profile 1 ($x = 0$) as a function of height z. Solid thick curve represents the time-averaged height-dependent fitting function of experimental flow velocity at Profile 1 (i.e., Eq. (S1) with $U_{max} = 6.451$ m/s, $z_u = 0.2751$ m, $\xi = 0.2374$, and $\chi = 3.6$). The values of u_{H1} used in the two-layer model are estimated from the parallel volume flux ($u_{H1}h_{H1}$) by integrating the fitting function of flow velocity from $z = 0$ to h_{H1} (gray region)

S2. Validation of the hindered-settling model for a dense underflow

In previous two-layer PDC models (e.g., Doyle et al. 2008; Kelfoun 2017; Shimizu et al. 2019), the basal layer of the stratified PDC is modeled as a dense underflow. In this Supplementary Information, the numerical result of our basal-layer model is compared with the experimental result of an initially fluidized granular flow (Girolami et al. 2008), where the sedimentation process has been successfully explained by hindered settling on the basis of a series of experiments (Girolami et al. 2010). We estimate the effective settling speed of particles at the bottom of the current (W_{sH}) that reproduces the experimental granular flow, and confirm that the estimated W_{sH} is explained by the hindered-settling model (i.e., Eq. (13) with $m = 2$–12).

In the numerical simulations, on the basis of the experimental setting, a stationary dense mixture in a rectangular-lock domain of length x_0 and height h_{H0} is released at time $t = 0$ and it flows into a one-dimensional horizontal channel (i.e., slope angle $\theta = 0°$) at $t > 0$. The dynamics of the dense current with thickness $h_{\mathrm{H}}(x, t)$ and velocity $u_{\mathrm{H}}(x, t)$ is described by the conservation equation of solid particle mass (i.e., Eq. (8) where the first term on the right-hand side is set to zero) and that of solid particle momentum (i.e., Eq. (9) where the third, fourth, and sixth terms on the right-hand side are set to zero). The aggradation rate of material in the deposits is given by Eqs. (10) and (11) where only the case of the aggradation from the lower layer is taken into account.

The values of input parameters (i.e., x_0, h_{H0}, ϕ_{sH}, ρ_{s}, and C_{db}) are determined by the experimental data at $t = 0$ and existing models (see Table S4). The length and thickness of the initial dense mixture (x_0 and h_{H0}) and the solid volume fraction in the dense current (ϕ_{sH}) are obtained from Table 2 of Girolami et al. (2015) under the additional assumption of $\phi_{\mathrm{sD}} = 0.6$. The mean solid density (ρ_{s}) is estimated by $\left(\sum\left(n_{\mathrm{s},i}/\rho_{\mathrm{s},i}\right)\right)^{-1}$, where $n_{\mathrm{s},i}$ and $\rho_{\mathrm{s},i}$ are the solid mass fraction and solid density for each i-th particle class obtained from the experimental data (Table 1 of Girolami et al. 2008 and Table 1 of Druitt et al. 2007). The basal-drag coefficient (C_{db}) is estimated on the basis of the empirical formula of Hager (1988) (i.e., $C_{\mathrm{db}} = 0.025 Re_{\mathrm{H0}}^{-0.2}$; cf. Hogg and Pritchard 2004), where $Re_{\mathrm{H0}} (\equiv \rho_{\mathrm{H}} U_{\mathrm{H}} h_{\mathrm{H0}} / \eta_{\mathrm{H}})$ is the representative Reynolds number of the dense current, $U_{\mathrm{H}} \left(\equiv \sqrt{\frac{\rho_{\mathrm{H}} - \rho_{\mathrm{a}}}{\rho_{\mathrm{H}}} g h_{\mathrm{H0}}}\right)$ is the representative flow velocity of the dense current, and the bulk dynamic viscosity of the dense current (η_{H}) is set to 10^{-5} Pa s on the basis of Thomas (1965). The values of the other input parameters (except for W_{sH}) are the same as those used in the numerical simulations of the two-layer PDC model (see Table 1).

In the numerical simulations, a dense current flows into the horizontal channel, and it produces the deposits by progressive aggradation at a constant deposition speed $D = \frac{\phi_{\mathrm{sH}}}{\phi_{\mathrm{sD}} - \phi_{\mathrm{sH}}} W_{\mathrm{sH}}$ (i.e., Eq. (11))

during flow (see Supplementary Movie 3 (ESM 5) for the results with $W_{\mathrm{sH}} = 7.3 \times 10^{-3}$ m/s (Table S4)); the dense current eventually stops its further propagation at the distal point where the horizontal mass flux of the current at the front becomes zero owing to basal deposition (cf. Shimizu et al. 2019). These features are consistent with the sedimentation process observed in the experiments (Girolami et al. 2008). The numerical results quantitatively reproduce the experimental data of the time-series of the flow front position (Fig. S2a) and that of the profile of the final deposit height (Fig. S2b) when W_{sH} is set to 7.3×10^{-3} m/s (Table S4).

The best-fit value ($W_{\mathrm{sH}} = 7.3 \times 10^{-3}$ m/s) is explained by the hindered-settling model as follows. The mean terminal velocity for the polydisperse system, $W_{\mathrm{T}} = \sum(n_{\mathrm{s},i} W_{\mathrm{T},i})$, is estimated to be 0.66 m/s on the basis of the experimental data (Table 1 of Girolami et al. 2008 and Table 1 of Druitt et al. 2007). Substituting this value into Eq. (13) with $m = 2-12$ and $\phi_{\mathrm{sH}} = 0.42$ yields $W_{\mathrm{sH}} = 9.6 \times 10^{-4}$–$2.2 \times 10^{-2}$ m/s, which includes the best-fit value of W_{sH}. This result suggests that W_{sH} based on the hindered-settling model can reproduce the dynamical features of the initially fluidized granular flow. Details of this experimental validation will be reported in future work.

Table S4 Input parameters and constants for simulation of the basal-layer model for initially fluidized granular flow

Variable	Value [unit]	Meaning
C_{db}	10^{-3}	Basal-drag coefficient of dense current
h_{H0}	0.25 [m]	Thickness of initial stationary dense mixture
W_{sH}	7.3×10^{-3} [m/s]	Settling speed at bottom of dense current
x_0	0.30 [m]	Length of initial stationary dense mixture
ρ_{s}	1474 [kg/m^3]	Mean density of solid particles
ϕ_{sH}	0.42	Mean volume fraction of solid particles in dense current

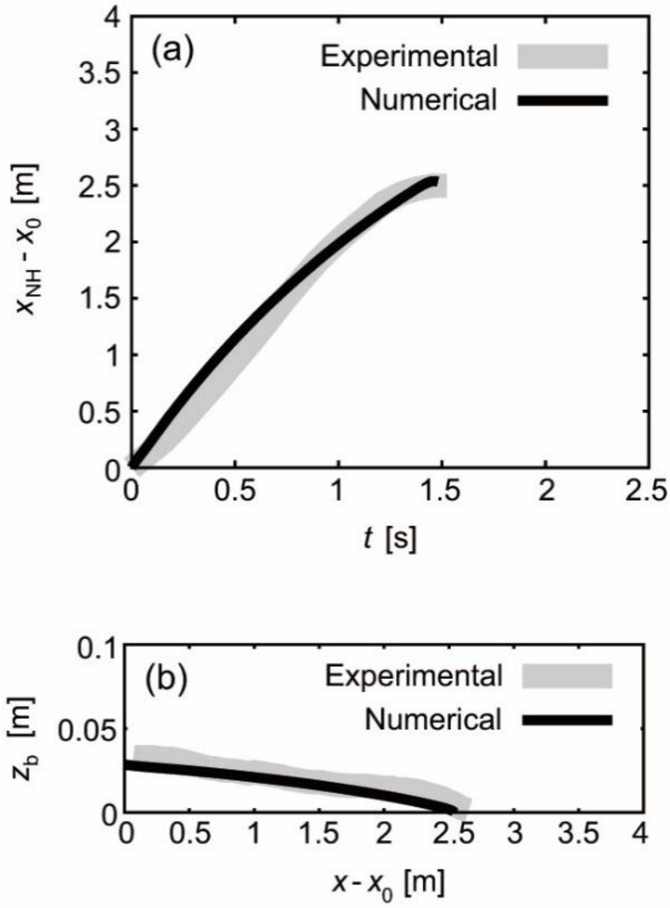

Fig. S2 Comparison of numerical results for the basal-layer model with $W_{\mathrm{sH}} = 7.3 \times 10^{-3}$ m/s (black curves) with experimental data for an initially fluidized granular flow (gray curves; Girolami et al. 2008). (a) Front position of the dense current as a function of time t ($x_{\mathrm{NH}}(t) - x_0$). The magnitude of typical errors in the experimental data is expressed by the thickness of the gray curve. (b) Final deposit height as a function of distance $x - x_0$ ($z_{\mathrm{b}}(x, t = \infty)$)

References

Brosch E, Lube G (2020) Spatiotemporal sediment transport and deposition processes in experimental dilute pyroclastic density currents. J Volcanol Geotherm Res 401:106946. https://doi.org/10.1016/j.jvolgeores.2020.106946

Cerminara M, Brosch E, Lube G (2021) A theoretical framework and the experimental dataset for benchmarking numerical models of dilute pyroclastic density currents. arXiv preprint. https://arxiv.org/abs/2106.14057

Doyle EE, Hogg AJ, Mader HM, Sparks RSJ (2008) Modeling dense pyroclastic basal flows from collapsing columns. Geophys Res Lett 35:L04305. https://doi.org/10.1029/2007GL032585

Druitt TH, Avard G, Bruni G, Lettieri P, Maez F (2007) Gas retention in fine-grained pyroclastic flow materials at high temperatures. Bull Volcanol 69(8):881–901. https://doi.org/10.1007/s00445-007-0116-7

Girolami L, Druitt TH, Roche O, Khrabrykh Z (2008) Propagation and hindered settling of laboratory ash flows. J Geophys Res 113:B02202. https://doi.org/10.1029/2007JB005074

Girolami L, Roche O, Druitt TH, Corpetti T (2010) Particle velocity fields and depositional processes in laboratory ash flows, with implications for the sedimentation of dense pyroclastic flows. Bull Volcanol 72(6):747–759. https://doi.org/10.1007/s00445-010-0356-9

Girolami L, Druitt TH, Roche O (2015) Towards a quantitative understanding of pyroclastic flows: Effects of expansion on the dynamics of laboratory fluidized granular flows. J Volcanol Geotherm Res 296:31–39. https://doi.org/10.1016/j.jvolgeores.2015.03.008

Hager WH (1988) Abflussformeln für turbulente Strömungen. Wasserwirtschaft 78:79–84

Hogg AJ, Pritchard D (2004) The effects of hydraulic resistance on dam-break and other shallow inertial flows. J Fluid Mech 501:179–212. https://doi.org/10.1017/S0022112003007468

Kelfoun K (2017) A two-layer depth-averaged model for both the dilute and the concentrated parts of pyroclastic currents. J Geophys Res 122:4293–4311. https://doi.org/10.1002/2017JB014013

Shimizu HA, Koyaguchi T, Suzuki YJ (2019) The run-out distance of large-scale pyroclastic density currents: A two-layer depth-averaged model. J Volcanol Geotherm Res 381:168–184. https://doi.org/10.1016/j.jvolgeores.2019.03.013

Thomas DG (1965) Transport characteristics of suspension: VIII. A note on the viscosity of Newtonian suspensions of uniform spherical particles. J Colloid Sci 20:267–277. https://doi.org/10.1016/0095-8522(65)90016-4